Theor Chem Acc (2014) 133:1586
DOI 10.1007/s00214-014-1586-2

REGULAR ARTICLE

Noncovalent interactions in dimers and trimers of SO_3 and CO

Luis Miguel Azofra · Ibon Alkorta · Steve Scheiner

Received: 28 August 2014 / Accepted: 10 October 2014 / Published online: 22 October 2014

Abstract The SO_3:CO heterodimer has been found by ab initio calculations to form a complex in which the C lone pair of CO interacts with the π*(SO) antibond via the π-hole lying directly above the S atom of SO_3. The binding energy of this complex is 4.3 kcal/mol, with Coulombic attraction as its main component. There is also a secondary minimum, with half that strength, wherein the CO molecule is rotated so that it is its O atom that interacts with SO_3. The most stable SO_3:$(CO)_2$ heterotrimer has the two CO molecules approaching the S atom from above and below the SO_3 plane with the C atoms of the CO interacting with the S of the SO_3. A strong chalcogen bond between SO_3 molecules is the dominant feature of the $(SO_3)_2$:CO trimer, supplemented by a S···C chalcogen bond in the SO_3:CO dimer.

Keywords Chalcogen bonds · S···C bonds · S···O bonds · π-Hole

1 Introduction

Noncovalent bonds [1], such as hydrogen [2–5], halogen [6–11], pnicogen [12–20] or tetrel [21–24] interactions, are essential ingredients in the structure adopted by bimolecular complexes and by numerous single molecules, as these bonds can represent large fractions of the forces between segments that are not directly covalently bonded to one another. Chalcogen bonds (YB) [25–38] are noncovalent interactions, which arise when an atom of the chalcogen family (Y), e.g., O, S, Se or Te, acting as Lewis acid, is drawn toward another electronegative atom, acting as Lewis base, due in part to the anisotropic distribution of electron density around Y [39]. The electrostatic attractions within these chalcogen bonds are supplemented by charge transfer from the lone pair(s) of the electron donor atom into the σ* or π* antibonding Z–Y orbitals (where Z is covalently bonded to Y), which tend to weaken and lengthen the latter Z–Y bond [40–43].

The present work examines the complexes formed between SO_3 and CO, as well as their 1:2 and 2:1 heterotrimers. Understanding the behavior of these molecules when interacting with one another is important to the basic knowledge of the various noncovalent forces. The work documents the primary attractive force to be a surprisingly strong chalcogen bond between a lone pair of the C (or O) atom of CO and the π-hole of SO_3 via its π*(SO) antibonding orbitals.

2 Computational details

The structure, energy and properties of the SO_3:CO heterodimers, and the SO_3:$(CO)_2$ and $(SO_3)_2$:CO heterotrimers, were studied through the use of the second-order Møller–Plesset perturbation theory (MP2) [44] with the aug-cc-pVTZ basis set [45, 46]. In all cases, vibrational frequencies were calculated in order to verify that the structures obtained correspond to true minima and to obtain the zero point vibrational energy (ZPE). Also, binding energies for the heterodimers were corrected by the counterpoise

Published as part of the special collection of articles derived from the 9th Congress on Electronic Structure: Principles and Applications (ESPA 2014).

L. M. Azofra (✉) · I. Alkorta
Instituto de Química Médica, CSIC, Juan de la Cierva, 3, 28006 Madrid, Spain
e-mail: luisazofra@iqm.csic.es

S. Scheiner
Department of Chemistry and Biochemistry, Utah State University, Logan, UT 84322-0300, USA

procedure [47]. All calculations were carried out via the GAUSSIAN09 program (revision D.01) [48].

Binding energies, E_b, were computed as the difference in energy between the complex on one hand and the sum of the energies of the isolated optimized monomers on the other. In order to obtain more accurate values, single point coupled-cluster CCSD(T) [49]/aug-cc-pV*X*Z (X = T, Q) calculations from the optimized MP2/aug-cc-pVTZ minima were performed via MOLPRO program [50].

The many-body procedure [51, 52] was applied to the trimers (Eq. 1) whereby the binding energy can be expressed as:

$$E_b = E_r + \Sigma\Delta^2 E + \Delta^3 E \quad (1)$$

where E_r represents the energy arising from the monomers' deformation and $\Delta^n E$ is the nth complex term (n = 2 for dimers and 3 for trimers). $\Delta^3 E$ represents the total cooperativity in the full trimer.

Atoms in molecules (AIM) [53, 54] theory at the MP2/aug-cc-pVTZ level, and natural bond orbital (NBO) [55] theory with the ωB97XD [56] functional and the aug-cc-pVTZ basis set, were applied to analyze the noncovalent interactions, using the AIMAll [57] and NBO6.0 [58] programs. The appearance of an AIM bond critical point (BCP) between centers of different monomers supports the presence of an attractive bonding interaction, which can also be examined by NBO charge transfer between orbitals of different fragments [53, 59].

The molecular electrostatic potential (MEP) on the 0.001 au electron density isosurface at MP2/aug-cc-pVTZ level was analyzed for the monomers via the WFA-SAS program [60]. Also, for the heterodimers, the electron density shift (EDS) maps were calculated as the difference between the electron density of the complex and the sum of those of the monomers in the geometry of the complex.

The interaction energy of each SO_3:CO heterodimer was decomposed via DFT-SAPT calculations at the PBE0 [61]/aug-cc-pVTZ level with the MOLPRO program [50]. The DFT-SAPT interaction energy, $E^{\text{DFT-SAPT}}$, is obtained as the sum of five components (Eq. 2): electrostatic (*ES*), exchange (*EX*), induction (*IND*), dispersion (*DISP*) and higher-order contributions (δ_{HF}) [62].

$$E^{\text{DFT-SAPT}} = ES + EX + IND + DISP + \delta_{HF} \quad (2)$$

3 Results and discussion

3.1 Monomers

Sulfur trioxide (SO_3) and carbon monoxide (CO) adopt D_{3h} and $C_{\infty v}$ symmetry, respectively. Their molecular electrostatic potential (MEP) on the 0.001 au electron density isosurface is illustrated in Fig. 1. The black dots represent maxima on the surface. In the case of SO_3, these maxima occur directly above and below the S atom, so may be referred to as π-holes. The cylindrical symmetry of CO leads to an equatorial belt of positive MEP around the middle of the molecule, represented by the series of black dots. The values of the MEP maxima for the SO_3 and CO molecules are 52.8 and 10.9 kcal/mol, respectively. The green dots indicate the positions of minima on the MEP. These points occur in the approximate positions of the O lone pairs in SO_3 and are rather shallow with a value of −9.0 kcal/mol. The minima occur on the two extensions of the CO axis, with the one on the C end somewhat more negative at −14.0 kcal/mol versus only −4.1 kcal/mol for the O terminus. The more negative C end is verified by the calculated dipole moment of CO, which is 0.254 D at MP2/aug-cc-pVTZ level, close to the experimental value of 0.11 D [63]. As described below, the positions of these extrema in the MEP act to guide the molecules into their respective dispositions in the dimers and trimers.

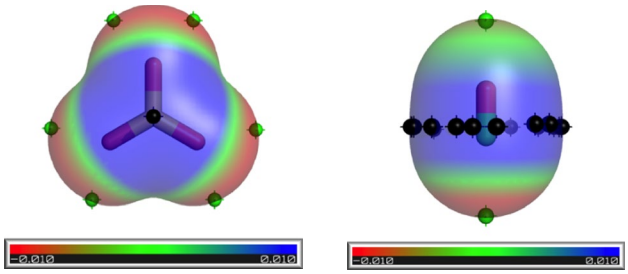

SO_3 (D_{3h}) CO ($C_{\infty v}$)

Fig. 1 Molecular electrostatic potential (MEP) on the 0.001 au electron density isosurface for the SO_3 and CO monomers, both calculated at the MP2/aug-cc-pVTZ level. The *red* and *blue colors* indicate negative and positive regions, respectively, varying between −0.010 and +0.010 au. *Black* and *green dots* indicate the location of the ESP maxima and minima, respectively, on the surface. The *black dots* for CO represent an equatorial belt of cylindrical symmetry

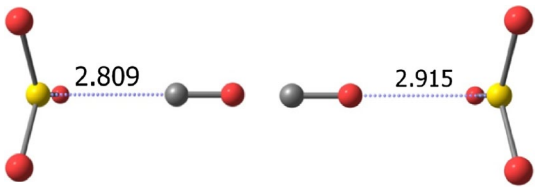

A1 (C_{3v}) **A2** (C_{3v})

Fig. 2 Structures of the two SO_3:CO heterodimers optimized at the MP2/aug-cc-pVTZ level. *Broken blue lines* connect interacting moieties corroborated by AIM. Interatomic distances in Å

3.2 SO_3:CO heterodimers

The potential energy surface (PES) of the SO_3:CO heterodimers contains two minima (see Fig. 2). CO approaches the S atom from above via its C atom in the more stable

Table 1 Binding energy, E_b, for the SO_3:CO heterodimers at the MP2/aug-cc-pVTZ and CCSD(T)/aug-cc-pVXZ (X = T, Q; single point) levels

Dimer	MP2				CCSD(T)[a]
	E_b^b	E_b + BSSE[c]	ΔH	ΔG	E_b
A1	−4.74 (−3.85)	−3.90	−3.69	3.57	−4.34 (−4.20)
A2	−2.15 (−1.69)	−1.56	−1.22	4.36	−2.47 (−2.26)

Also, enthalpy, ΔH, and Gibbs free energy, ΔG, for the association reactions at room temperature (298 K) and at MP2/aug-cc-pVTZ computational level are shown. All quantities in kcal/mol

[a] CCSD(T)/aug-cc-pVTZ//MP2/aug-cc-pVTZ and, in parentheses, CCSD(T)/aug-cc-pVQZ//MP2/aug-cc-pVTZ computational levels

[b] Zero point vibrational energy corrections (ZPE) added in parentheses

[c] Basis set superposition error (BSSE)

Table 2 Natural bond orbital parameters [$E(2)$ in kcal/mol] at ωB97XD/aug-cc-pVTZ level, and AIM descriptors (electron density, ρ_{BCP}, and its Laplacian at the BCP, both in au) at MP2/aug-cc-pVTZ computational level for the noncovalent interactions present in the indicated dimers and **B1**–**B3** trimers

Complex	NBO		AIM	
	Donor lone pair	$E(2)$	ρ_{BCP}	$\nabla^2\rho_{BCP}$
A1	C	6.24	0.020	0.055
A2	O	1.10	0.010	0.045
B1	C, C	5.40, 5.40	0.016, 0.016	0.049, 0.049
B2	C, O	6.20, 1.17	0.019, 0.009	0.052, 0.041
B3	O, O	1.21, 1.21	0.010, 0.010	0.044, 0.044

Sum of all the $C_{lp}/O_{lp} \rightarrow \pi^*(SO)$ components for a same type interaction

complex, **A1**, while the approach is via the O atom in **A2**. In either case, the interactions can be described as the approach of a negative minimum in the MEP of CO toward the positive π-hole above S. The greater stability of **A1** is consistent with the more negative minimum near the C atom, as well as the 0.1 Å shorter intermolecular distance. No dimers in which the O lone pairs from SO_3 interact with the positive belt in CO have found, due to the very poor electrostatic power of this last region.

The energetics of the two complexes are displayed in Table 1 which shows the binding energy of **A1** to be roughly twice that of **A2**, both before and after zero point energies basis set superposition errors (BSSE) are added in. Raising the level of correlation from MP2 to CCSD(T) reduces the binding energy of **A1** and raises that of **A2**, but by small amounts in either case. As can be seen in Table 1 about E_b at CCSD(T) level, small differences arise from the change in the aug-cc-pVTZ and aug-cc-pVQZ basis sets. The more stable OC···SO_3 complex is bound by approximately the same amount as the water dimer [64], the paradigm of classic H-bonding. The succeeding columns indicate that ΔH is rather similar to the ZPE-corrected binding energy. ΔG, on the other hand, is positive at 298 K, less so for **A1** than for **A2**. This thermodynamic quantity is negative for temperatures below −121 K for **A1**, and below −208 K for **A2**.

In addition to a simple electrostatic attraction, Table 2 reports measures of a stabilizing charge transfer between the two molecules. The NBO value of $E(2)$ represents an energetic assessment of the charge transfer from the C/O lone pair of CO in **A1/A2**, to a π* antibonding orbital of SO_3. There is a fairly large $E(2)$ of 6.24 kcal/mol for **A1**, and a smaller but still significant $E(2)$ of 1.10 kcal/mol for **A2**. The last two columns of Table 2 present the values of the electron density ρ and its Laplacian $\nabla^2\rho$ at the C/O···S bond critical point as determined by AIM analysis. Consistent with the other trends, both of these measures of bond strength are larger for **A1** than for **A2**.

The decomposition of the total interaction energy into its constituent parts was calculated via DFT-SAPT, and the results are reported in Table 3. The electrostatic force represents the strongest attractive component for **A1**, followed by dispersion and then by induction. Electrostatic is much smaller in **A2** and is in fact surpassed by dispersion, with induction again playing a much more minor role. The smaller Coulombic attraction in **A2** is understandable based on the CO dipole moment, which is repelled by the SO_3 quadrupole moment.

Another result of the formation of a dimer is the shift of electron density that accompanies the complexation. These shifts are displayed in Fig. 3 where electron density increments are denoted in purple and losses in green. The patterns for both **A1** and **A2** are similar, but again they are attenuated in **A2**. A gain is observed in the C/O atom that is approaching the SO_3 molecule from above, and a loss on the other atom of CO. This pattern is verified by NBO atomic charges wherein the atom of CO interacting directly with SO_3 acquires additional charge, at the expense of the other atom. There is an internal shift of density from the region immediately above the S atom of SO_3 toward the three O atoms, a redistribution consistent with the NBO atomic charges. It would appear from Fig. 3 that the latter internal polarization of SO_3 is considerably smaller in **A2,** while the changes within CO are fairly similar from **A1** to **A2**, again all consonant with NBO atomic charge patterns. In terms of the amount of charge transferred between molecules, from CO to SO_3, both Fig. 3 and the NBO atomic charges suggest that there is very little transfer in **A2**, as most of the density rearrangement is internal, particularly within CO.

Dipole moments of the complexes also reflect charge redistribution. The dipole of the CO monomer is 0.254 D, in the $^-$C–O$^+$ direction. This moment is increased more

Table 3 Interaction energy components (kcal/mol) for the SO_3:CO heterodimers, calculated using the DFT-SAPT (PBE0/aug-cc-pVTZ) methodology

Complex	*ES*	*EX*	*IND*	*DISP*	δ_{HF}	$E^{DFT\text{-}SAPT}$
A1	−7.62	12.00	−2.13	−4.15	−1.40	−3.30
A2	−2.01	3.26	−0.55	−2.12	−0.28	−1.70

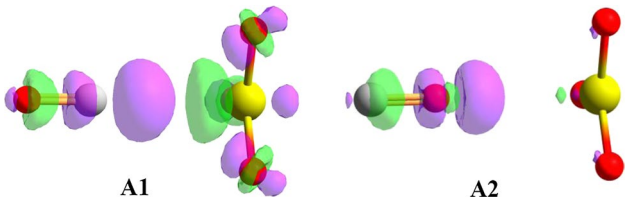

Fig. 3 Electron density shifts in SO_3:CO dimers caused by formation of complex. Contours represent the ±0.001 au surface; increase in *purple* and decrease in *green*

Table 4 Changes in internal bond lengths (mÅ) and vibrational frequencies (cm^{-1}) of monomers upon formation of dimers and **B1**-**B3** trimers

Complex	R(C≡O)	ν(C≡O)	R(S=O)	ν_{st}(S=O)[a]
A1	−2.5	21	−1.7	10
A2	0.8	−2	1.0	−4
B1	−1.9	16, 16	−2.2	16
B2	−2.5, 0.5	20, −1	−2.2	13
B3	0.8	−3, −3	−1.4	7

In monomers, R(C≡O) = 1.1390 Å and ν(C≡O) = 2,110 cm^{-1}; R(S=O) = 1.4451 Å, ν_{st} = 1,036 cm^{-1}

[a] Symmetric stretching frequency

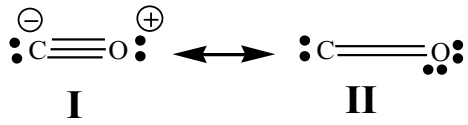

Scheme 1 Lewis structure analysis in the CO monomer

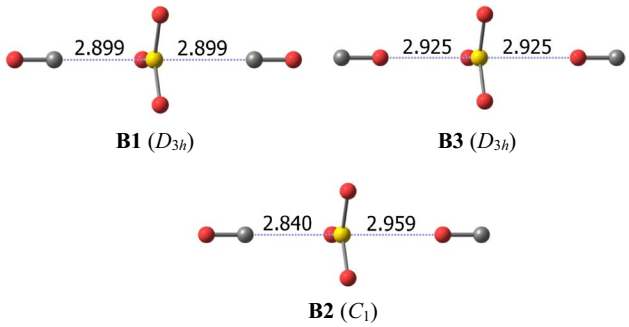

Fig. 4 Structures of the SO_3:$(CO)_2$ heterotrimers optimized at the MP2/aug-cc-pVTZ level. *Broken blue lines* connect interacting moieties corroborated by AIM. Interatomic distances in Å

than fourfold in complex **A1**, which is consistent with the shift of density from O to C in Fig. 3. This same figure shows the opposite polarization, from C to O, in **A2**. This polarization indeed reverses the dipole of CO, to $^{+}C–O^{-}$, with a magnitude of 0.149 D.

Even weak noncovalent interactions are known to induce perturbations in the internal properties of the monomers. Table 4 lists the changes in the internal bond lengths and vibrational frequencies that occur upon forming dimers **A1** and **A2**. It is first notable that these two structures influence the monomers in opposite ways. In structure **A1**, the bonds of both molecules become shorter and the frequencies shift to the blue. The changes are of opposite sign in **A2** and smaller in magnitude.

There are perhaps several ways to understand these trends. With respect to CO, the largest shift in orbital occupancy upon forming the **A1** dimer is a 28 me drop in the C lone pair orbital. A pictorial examination of this orbital shows a node in the region between the C and O atoms, which may be characterized as antibonding character. The loss of density from this orbital may thus be associated with an enhanced C–O bond strength, which leads to the observed bond contraction and blue shift. The loss of occupancy of the O lone pair in **A2** is very small, less than 1 me, so is consistent with the very small changes in the CO bond strength markers in Table 4.

Another and less rigorous manner of understanding these patterns is associated with a simple Lewis structure analysis. One may consider the bonding of CO to consist of a resonance between a triple-bonded structure I with opposite charges on the two atoms, as shown in Scheme I, and II which contains two neutral atoms connected by a double bond (see Scheme 1). The shift in charge which amplifies the charge separation in **A1** would tend to push the equilibrium between I and II toward I, and the stronger triple bond contained therein.

3.3 SO_3:$(CO)_2$ heterotrimers

Upon adding a second CO monomer to the SO_3:CO dimer, the potential energy surface was searched in two steps: (1)

Table 5 Many-body analysis (kcal/mol) for the SO_3:$(CO)_2$ heterotrimers calculated at MP2/aug-cc-pVTZ level

Comp.	E_r	E_{12}	E_{13}	E_{23}	$\Sigma\Delta^2E$	Δ^3E	E_b
B1	0.03	−4.65	−4.65	−0.01	−9.31	0.55	−8.73
B2	0.07	−4.79	−2.14	−0.01	−6.94	0.22	−6.64
B3	0.00	−2.15	−2.15	−0.06	−4.36	0.05	−4.31

Subscripts 1, 2 and 3 refer to SO_3, CO(1), and the second CO monomer [CO(2)], respectively. Binding energies in **A1** and **A2** dimers are −4.74 and −2.15 kcal/mol, respectively

using the **A1** and **A2** dimers as starting points and (2) beginning with fresh initial starting points. For this second purpose, the coalescence-kick program was employed, which provides a fully objective searching protocol [65]. The three minima in Fig. 4 resulted from this combined approach. All three resemble the dimers in that the CO molecules approach SO_3 both from above and below. In the most stable **B1**, S is attacked by C atoms, by O atoms in **B3**, and by one of each in **B2**. The order of stability follows the dimer pattern that the C atom is favored over O to form a S···C chalcogen bond. The very weak interactions between CO monomers precluded formation of SO_3:$(CO)_2$ heterotrimers where a pair of CO molecules interact with one another. Indeed, $(CO)_2$ homodimers are described in the literature as bound by only very weak van der Waals bonds [66–68].

There is evidence of negative cooperativity in the S···X bond lengths. Whereas R(S···C) = 2.809 Å in **A1**, it is elongated in the trimers; likewise, the S···O bonds in the trimers are longer that its value of 2.915 Å in **A2**. This mutual weakening effect may be understood first on the basis that SO_3 serves as double electron acceptor in the trimers. A related description might utilize the weakening of the SO_3 π-hole upon its complexation with the first CO molecule. For example, the π-hole in the SO_3 monomer has a magnitude of 52.8 kcal/mol, which is reduced to 44.6 in **A1** and 50.8 in **A2**.

Other evidence of antagonistic behavior is observed in the electronic structure. It may be noted from Table 2 that the $E(2)$ $C_{lp} \rightarrow \pi^*(SO)$ charge transfer energy of the **A1** dimer of 6.24 kcal/mol is reduced in the trimers, although there is a slight rise in the $O_{lp} \rightarrow \pi^*(SO)$ quantities. The AIM measures in the last two columns also show a bond weakening upon going from dimer to trimer.

The changes in the internal parameters provide further support of negative cooperativity. The CO bond length contraction of 2.5 mÅ in **A1** is reduced in **B1**, and the 0.8 mÅ stretch in **A2** is lowered to 0.5 in **B2**, with similar patterns noted in ν(C≡O). On the other hand, the 1.7 mÅ contraction of R(S=O) in **A1** is amplified to 2.2 mÅ in **B1** and **B2**, suggesting that the effects of one CO molecule upon the central SO_3 are enhanced by a second CO on the other side of the trimer. This same amplification is observed in the symmetric SO stretching frequency.

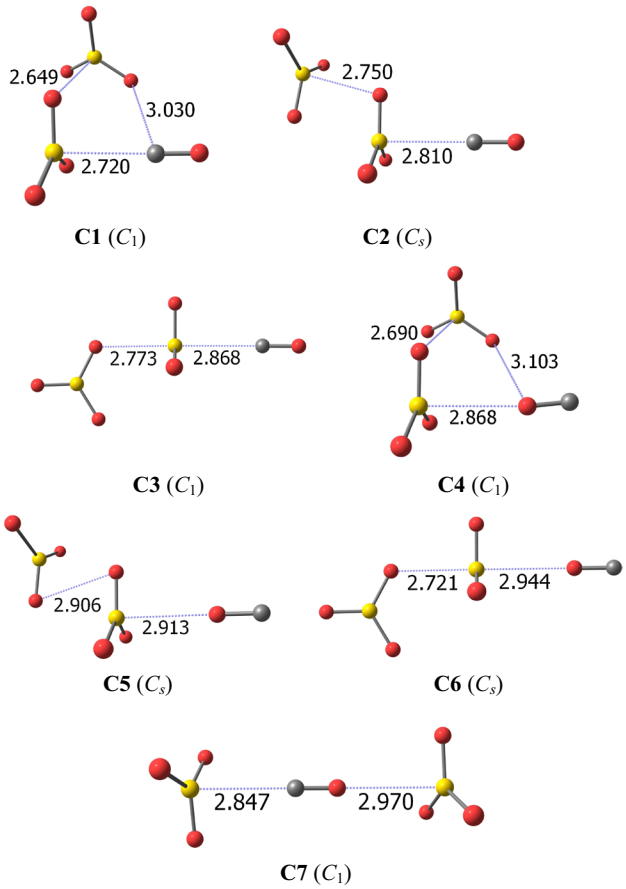

Fig. 5 Structures of $(SO_3)_2$:CO heterotrimers optimized at the MP2/aug-cc-pVTZ level. *Broken blue lines* connect interacting moieties corroborated by AIM. Interatomic distances in Å

The many-body analysis for the SO_3:$(CO)_2$ heterotrimers reported in Table 5 shows first that the interaction energies of the **A1** and **A2** dimers are changed very little when placed in the context of pairwise interactions E_{12} and E_{13} in the trimers. The small changes in the geometry have a negligible energetic effect, as is clear from the very small values of E_r in the first column of Table 5. The third-order term, Δ^3E, which represents the total cooperativity is positive in all cases, again confirming the negative cooperativity. Note that this term is largest for the most strongly bound trimers.

3.4 $(SO_3)_2$:CO heterotrimers

As for the SO_3:$(CO)_2$ complexes, the inclusion of a second SO_3 monomer was performed: (1) through the **A1** and **A2** dimers and (2) beginning with fresh initial starting points. SO_3 molecules can engage in relatively strong noncovalent bonds [37]. For that reason, the six most stable minima of the seven found on the $(SO_3)_2$:CO potential energy surface in Fig. 5 include stabilizing interactions between the SO_3 monomers. Structure **C1**, for example, includes a S···O chalcogen bond between SO_3 molecules as the shortest contact, as well as a S···C contact reminiscent of that in dimer **A1**, and a longer C···O contact. Structure **C1**, like **C4**, could best be described as a cyclic geometry. In **C2**, **C3**, and **C5**, SO_3 occupies a central position, whereas CO is located between the two SO_3 molecules in **C7**.

The changes induced in the CO monomer by formation of these heterotrimers are documented in Table 6. There is a clear pattern of CO bond contraction and blue shifts in **C1**, **C2**, **C3**, and **C7**, with opposite, albeit smaller, changes in **C4**–**C6**. Consistent with the results for the dimers, the former set of trimers all involves interaction of the C atom of CO, while the O atom participates in the bonding in the latter set.

Table 6 Changes in internal bond lengths (mÅ) and vibrational frequencies (cm^{-1}) of monomers upon formation of dimers and **C1**–**C7** trimers

Complex	R(C≡O)	ν(C≡O)
C1	−3.3	27
C2	−2.7	22
C3	−2.2	18
C4	1.0	−3
C5	0.8	−3
C6	0.6	−2
C7	−1.8	19

In monomers, R(C≡O) = 1.1390 Å and ν(C≡O) = 2,110 cm^{-1} ; R(S=O) = 1.4451 Å, ν_{st} = 1,036 cm^{-1}

The many-body analysis of the seven $(SO_3)_2$:CO heterotrimers in Table 7 shows first that the distortion energy remains low, here less than 0.4 kcal/mol. Again, the bimolecular terms representing OC···SO_3 and CO···SO_3 interactions are quite similar to their values in the **A1** and **A2** dimers. While generally small, the cooperativity term Δ^3E is negative in many cases, indicating a synergistic effect, but especially large in **C1**. Not surprisingly, positive values of Δ^3E are characteristic of structures where the central molecule plays the role of either double electron acceptor (**C3** and **C6**) or donor (**C7**).

Due in part to their cyclic nature, the structure of NBO charge transfers in the $(SO_3)_2$:CO heterotrimers is more complicated than in those of the preceding structures. The values of $E(2)$ are displayed in Table 8, along with their donor and acceptor orbitals. The stability of **C1** can be traced to a pair of important transfers. The largest is the $C_{lp} \rightarrow \pi^*$(SO) transfer involving CO, followed closely by an $O_{lp} \rightarrow \pi^*$(SO) chalcogen bond between two SO_3 molecules. And indeed, these $C_{lp} \rightarrow \pi^*$(SO) transfers are typically more substantial than the chalcogen bonds between SO_3 molecules. As in the dimers, the $C_{lp} \rightarrow \pi^*$(SO) values of $E(2)$ are consistently much larger than $O_{lp} \rightarrow \pi^*$(SO).

Another manifestation of the synergistic effects in some of these trimers can be seen in the values of $C_{lp} \rightarrow \pi^*$(SO) $E(2)$, which was equal to 6.24 kcal/mol in **A1**. This quantity exceeds this value in **C1** and **C2**. In both of these structures, the second SO_3 molecule engages in a S···O chalcogen bond with the first SO_3, which retrieves electron density from it, and thereby enhancing its π-hole, and also permitting a larger charge transfer from the C lone pair.

4 Summary

The C atom of CO attacks the SO_3 molecule from directly above the SO_3 plane, to form a S···C chalcogen bond. This interaction is largely electrostatic in nature, with the negative end of the CO dipole advancing toward the π-hole that lies above the S atom. It is supplemented by the charge

Table 7 Many-body analysis (kcal/mol) for the $(SO_3)_2$:CO heterotrimers calculated at the MP2/aug-cc-pVTZ level

Comp.	E_r	E_{12}	E_{13}	E_{23}	$\Sigma\Delta^2E$	Δ^3E	E_b
C1	0.39	−4.78	−4.82	−1.01	−10.60	−0.86	−11.08
C2	0.18	−4.90	−4.77	−0.20	−9.87	−0.09	−9.78
C3[a]	0.08	−4.60	−0.03	−4.71	−9.34	0.38	−8.89
C4	0.14	−4.75	−2.11	−0.75	−7.61	−0.26	−7.73
C5	0.14	−5.03	−2.14	−0.07	−7.24	−0.02	−7.12
C6	0.11	−4.73	−0.06	−2.14	−6.93	0.13	−6.69
C7	0.05	−4.76	0.10	−2.13	−6.79	0.40	−6.35

Subscripts 1, 2 and 3 refer to $SO_3(1)$, the second SO_3 monomer [$SO_3(2)$], and the CO monomer, respectively

[a] **C3** contains one very small imaginary frequency of 8*i* cm^{-1}

Table 8 NBO values of E(2) (kcal/mol) at the ωB97XD/aug-cc-pVTZ level for the noncovalent interactions present in the $(SO_3)_2$:CO heterotrimers

Complex	Donor/Acc.	Type	$E(2)$
C1	$SO_3(2)/SO_3(1)$	$O_{lp} \rightarrow \pi^*(SO)$	10.74
	$SO_3(1)/CO$	$O_{lp} \rightarrow \pi^*(CO)$	0.69
	$CO/SO_3(1)$	$C_{lp} \rightarrow \pi^*(SO)$	11.39
C2	$SO_3(2)/SO_3(1)$	$O_{lp} \rightarrow \pi^*(SO)$	4.46
	$SO_3(1)/SO_3(2)$	$O_{lp} \rightarrow \pi^*(SO)$	2.58
	$CO/SO_3(1)$	$C_{lp} \rightarrow \pi^*(SO)$	7.24
C3	$SO_3(2)/SO_3(1)$	$O_{lp} \rightarrow \pi^*(SO)$	4.55
	$CO/SO_3(1)$	$C_{lp} \rightarrow \pi^*(SO)$	5.79
C4	$SO_3(2)/SO_3(1)$	$O_{lp} \rightarrow \pi^*(SO)$	4.90
	$CO/SO_3(1)$	$O_{lp} \rightarrow \pi^*(SO)$	0.59
C5	$SO_3(2)/SO_3(1)$	$O_{lp} \rightarrow \pi^*(SO)$	3.38
	$SO_3(1)/SO_3(2)$	$O_{lp} \rightarrow \pi^*(SO)$	3.26
	$CO/SO_3(1)$	$O_{lp} \rightarrow \pi^*(SO)$	1.34
C6	$SO_3(2)/SO_3(1)$	$O_{lp} \rightarrow \pi^*(SO)$	5.14
	$CO/SO_3(1)$	$O_{lp} \rightarrow \pi^*(SO)$	1.16
C7	$CO/SO_3(1)$	$C_{lp} \rightarrow \pi^*(SO)$	5.93
	$CO/SO_3(2)$	$O_{lp} \rightarrow \pi^*(SO)$	0.83

$SO_3(1)$ and $SO_3(2)$ refer to the derived and nonderived SO_3 structure in dimers for the $(SO_3)_2$:CO heterotrimers, in each case

transfer from the C lone pair into the π*(SO) antibonding system, as well as a sizable dispersion contribution. In total, the binding energy of this heterodimer is between 4 and 5 kcal/mol, similar to the H-bond energy of the water dimer. A secondary minimum occurs if the CO molecule is rotated around so that its O atom attacks the S of SO_3, but this structure is more weakly bound.

This same S···O chalcogen bond is the guiding feature in the global minimum of the SO_3:$(CO)_2$ heterotrimer. The C atoms of the two CO molecules simultaneously approach the S of SO_3 from above and below. This assembly leads to a minor degree of negative cooperativity, as the central SO_3 molecule serves as double electron acceptor. In the case of the $(SO_3)_2$:CO trimer, there are two strong noncovalent bonds present. In the first place, there is the same S···C chalcogen bond that is the common feature of the dimer. This interaction is supplemented by an equally strong S···O chalcogen bond between the pair of SO_3 molecules. Due to its cyclic structure, with each of the three molecules acting as both electron donor and acceptor, this complex exhibits a synergistic positive cooperativity that amounts to nearly 1 kcal/mol.

In addition to the global minima, the potential energy surface of each heterotrimer contains a number of secondary minima as well. The stability of each can be explained on the basis of charge transfers and alignment of positive with negative extremes of the molecular electrostatic potentials.

Acknowledgments This work has been supported by the CTQ2012–35513–C02–02 (MINECO) project. LMA thanks the MICINN for a PhD grant (No. BES–2010–031225). Computer, storage and other resources from the CTI (CSIC) and from the Division of Research Computing in the Office of Research and Graduate Studies at Utah State University are gratefully acknowledged.

References

1. Hobza P, Müller-Dethlefs K (2009) Non-covalent interactions. The Royal Society of Chemistry, Cambridge
2. Schuster P, Zundel G, Sandorfy C (1976) The hydrogen bond. Recent developments in theory and experiments. North-Holland Publishing Co., Amsterdam
3. Scheiner S (1997) Hydrogen bonding: a theoretical perspective. Oxford University Press, New York
4. Grabowski SJ (2006) Hydrogen bonding—new insights. Springer, Dordrecht
5. Gilli G, Gilli P (2009) The nature of the hydrogen bond. Oxford University Press, Oxford
6. Lommerse JPM, Stone AJ, Taylor R, Allen FH (1996) J Am Chem Soc 118:3108–3116
7. Metrangolo P, Resnati G (2008) Science 321:918–919
8. Zierkiewicz W, Michalska D, Zeegers-Huyskens T (2010) Phys Chem Chem Phys 12:13681–13691
9. Adhikari U, Scheiner S (2012) Chem Phys Lett 532:31–35
10. Politzer P, Murray JS, Clark T (2013) Phys Chem Chem Phys 15:11178–11189
11. Solimannejad M, Malekani M, Alkorta I (2013) J Phys Chem A 117:5551–5557
12. Tschirschwitz S, Lonnecke P, Hey-Hawkins E (2007) Dalton Trans 14:1377–1382
13. Bühl M, Kilian P, Woollins JD (2011) ChemPhysChem 12:2405–2408
14. Del Bene JE, Alkorta I, Sanchez-Sanz G, Elguero J (2011) Chem Phys Lett 512:184–187
15. Scheiner S (2011) J Phys Chem A 115:11202–11209
16. Zahn S, Frank R, Hey-Hawkins E, Kirchner B (2011) Chem Eur J 17:6034–6038
17. Adhikari U, Scheiner S (2012) Chem Phys Lett 536:30–33
18. Scheiner S (2012) Acc Chem Res 46:280–288
19. Alkorta I, Elguero J, Del Bene JE (2013) J Phys Chem A 117:4981–4987
20. Azofra LM, Alkorta I, Elguero J (2014) ChemPhysChem. doi:10.1002/cphc.201402086
21. Alkorta I, Rozas I, Elguero J (2001) J Phys Chem A 105:743–749
22. Azofra LM, Altarsha M, Ruiz-López MF, Ingrosso F (2013) Theor Chem Acc 132:1326
23. Bauzá A, Mooibroek TJ, Frontera A (2013) Angew Chem Int Ed 52:12317–12321
24. Grabowski SJ (2014) Phys Chem Chem Phys 16:1824–1834
25. Minyaev RM, Minkin VI (1998) Can J Chem 76:776–788
26. Rosenfield RE, Parthasarathy R, Dunitz JD (1977) J Am Chem Soc 99:4860–4862
27. Burling FT, Goldstein BM (1992) J Am Chem Soc 114:2313–2320
28. Iwaoka M, Takemoto S, Tomoda S (2002) J Am Chem Soc 124:10613–10620
29. Werz DB, Gleiter R, Rominger F (2002) J Am Chem Soc 124:10638–10639
30. Bleiholder C, Werz DB, Köppel H, Gleiter R (2006) J Am Chem Soc 128:2666–2674
31. Sánchez-Sanz G, Alkorta I, Elguero J (2011) Mol Phys 109:2543–2552

32. Jabłoński M (2012) J Phys Chem A 116:3753–3764
33. Sánchez-Sanz G, Trujillo C, Alkorta I, Elguero J (2012) ChemPhysChem 13:496–503
34. Adhikari U, Scheiner S (2014) J Phys Chem A 118:3183–3192
35. Azofra LM, Scheiner S (2014) J Phys Chem A 118:3835–3845
36. Azofra LM, Alkorta I, Scheiner S (2014) J Chem Phys 140:244311
37. Azofra LM, Alkorta I, Scheiner S (2014) Phys Chem Chem Phys 16:18974–18981
38. Bauzá A, Alkorta I, Frontera A, Elguero J (2013) J Chem Theory Comput 9:5201–5210
39. Cavallo G, Metrangolo P, Pilati T, Resnati G, Terraneo G (2014) Cryst Growth Des 14:2697–2702
40. Goettel JT, Chaudhary P, Hazendonk P, Mercier HPA, Gerken M (2012) Chem Commun 48:9120–9122
41. Murray J, Lane P, Clark T, Riley K, Politzer P (2012) J Mol Model 18:541–548
42. Azofra LM, Scheiner S (2014) J Chem Phys 140:034302
43. Azofra LM, Scheiner S (2014) Phys Chem Chem Phys 16:5142–5149
44. Møller C, Plesset MS (1934) Phys Rev 46:618–622
45. Dunning THJ (1989) J Chem Phys 90:1007–1023
46. Woon DE, Dunning TH (1993) J Chem Phys 98:1358–1371
47. Boys SF, Bernardi F (1970) Mol Phys 19:553–566
48. Frisch MJ, Trucks GW, Schlegel HB, Scuseria GE, Robb MA, Cheeseman JR, Scalmani G, Barone V, Mennucci B, Petersson GA, Nakatsuji H, Caricato M, Li X, Hratchian HP, Izmaylov AF, Bloino J, Zheng G, Sonnenberg JL, Hada M, Ehara M, Toyota K, Fukuda R, Hasegawa J, Ishida M, Nakajima T, Honda Y, Kitao O, Nakai H, Vreven T, Montgomery J, J. A., Peralta JE, Ogliaro F, Bearpark M, Heyd JJ, Brothers E, Kudin KN, Staroverov VN, Kobayashi R, Normand J, Raghavachari K, Rendell A, Burant JC, Iyengar SS, Tomasi J, Cossi M, Rega N, Millam NJ, Klene M, Knox JE, Cross JB, Bakken V, Adamo C, Jaramillo J, Gomperts R, Stratmann RE, Yazyev O, Austin AJ, Cammi R, Pomelli C, Ochterski JW, Martin RL, Morokuma K, Zakrzewski VG, Voth GA, Salvador P, Dannenberg JJ, Dapprich S, Daniels AD, Farkas Ö, Foresman JB, Ortiz JV, Cioslowski J, Fox DJ, GAUSSIAN09, Revision D.01, Wallingford CT, 2009
49. Pople JA, Head-Gordon M, Raghavachari K (1987) J Chem Phys 87:5968–5975
50. Werner H-J, Knowles PJ, Manby FR, Schütz M, Celani P, Knizia G, Korona T, Lindh R, Mitrushenkov A, Rauhut G, Adler TB, Amos RD, Bernhardsson A, Berning A, Cooper DL, Deegan MJO, Dobbyn AJ, Eckert F, Goll E, Hampel C, Hesselmann A, Hetzer G, Hrenar T, Jansen G, Köppl C, Liu Y, Lloyd AW, Mata RA, May AJ, McNicholas SJ, Meyer W, Mura ME, Nicklaß A, Palmieri P, Pflüger K, Pitzer R, Reiher M, Shiozaki T, Stoll H, Stone AJ, Tarroni R, Thorsteinsson T, Wang M, Wolf A, MOLPRO 2012.1, 2012
51. Xantheas SS, Dunning TH (1993) J Chem Phys 99:8774–8792
52. Xantheas SS (1994) J Chem Phys 100:7523–7534
53. Bader RFW (1990) Atoms in molecules: a quantum theory. Clarendon Press, Oxford
54. Popelier PLA (2000) Atoms in molecules. An introduction. Prentice Hall, Harlow
55. Weinhold F, Landis CR (2005) Valency and bonding. A natural bond orbital donor-acceptor perspective. Cambridge Press, Cambridge
56. Chai J-D, Head-Gordon M (2008) Phys Chem Chem Phys 10:6615–6620
57. Keith TA, AIMAll (Version 13.11.04), Overland Park KS, USA, 2013
58. Glendening ED, Badenhoop JK, Reed AE, Carpenter JE, Bohmann JA, Morales CM, Landis CR, Weinhold F, NBO 6.0, Madison, USA, 2013
59. Rozas I, Alkorta I, Elguero J (2000) J Am Chem Soc 122:11154–11161
60. Bulat F, Toro-Labbé A, Brinck T, Murray J, Politzer P (2010) J Mol Model 16:1679–1691
61. Perdew JP, Burke K, Ernzerhof M (1996) Phys Rev Lett 77:3865–3868
62. Chałasiński G, Szczęśniak MM (2000) Chem Rev 100:4227–4252
63. Muenter JS (1975) J Mol Spectrosc 55:490–491
64. Reimers JR, Watts RO, Klein ML (1982) Chem Phys 64:95–114
65. Sergeeva AP, Averkiev BB, Zhai H-J, Boldyrev AI, Wang L-S (2011) J Chem Phys 134:224304
66. van der Pol A, van der Avoird A, Wormer PES (1990) J Chem Phys 92:7498–7504
67. Brookes MD, McKellar ARW (1999) J Chem Phys 111:7321–7328
68. Vissers GWM, Wormer PES, van der Avoird A (2003) Phys Chem Chem Phys 5:4767–4771